

Observational Study

e Computerized Characterization of Spinal Structures on MRI and Clinical Significance of 3D Reconstruction of Lumbosacral Intervertebral Foramen

Zheng Liu, PhD¹, Zhihai Su, PhD¹, Min Wang, MD¹, Tao Chen, PhD¹, Zhifei Cui, MD¹, Xiaojun Chen, MD², Shaolin Li, MD², Qianjin Feng, PhD³, Shumao Pang, PhD³, and Hai Lu, PhD¹

From: ¹Fifth Affiliated Hospital of Sun Yat-sen University, Spinal surgery, Zhuhai, Guangdong, China; ²Fifth Affiliated Hospital of Sun Yat-sen University, Radiology, Zhuhai, Guangdong, China; ³Southern Medical University, School of Biomedical Engineering, Guangdong Provincial Key Laboratory of Medical Image Processing, Guangzhou, Guangdong, China

Address Correspondence:
Hai Lu, PhD

The Fifth Affiliated Hospital of Sun Yat-sen University
E-mail: lvhai@mail.sysu.edu.cn

Disclaimer: See pg. 33 for funding information of this study.

Conflict of interest: Each author certifies that he or she, or a member of his or her immediate family, has no commercial association (i.e., consultancies, stock ownership, equity interest, patent/licensing arrangements, etc.) that might pose a conflict of interest in connection with the submitted manuscript.

Manuscript received: 05-18-2021
Revised manuscript received: 09-08-2021
Accepted for publication: 09-14-2021

Free full manuscript:
www.painphysicianjournal.com

Background: Segmentation of spinal structures is important in medical imaging analysis, which facilitates surgeons to plan a preoperative trajectory for the transforaminal approach. However, manual segmentation of spinal structures is time-consuming, and studies have not explored automatic segmentation of spinal structures at the L5/S1 level.

Objectives: This study sought to develop a new method based on a deep learning algorithm for automatic segmentation of spinal structures. The resulting algorithm may be used to rapidly generate a precise 3D lumbosacral intervertebral foramen model to assist physicians in planning an ideal trajectory in L5/S1 lumbar transforaminal radiofrequency ablation (LTRFA).

Study Design: This was an observational study for developing a new technique on spinal structures segmentation.

Study site: The study was carried out at the department of radiology and spine surgery at our hospital.

Methods: A total of 100 L5/S1 level data samples from 100 study patients were used in this study. Masks of vertebral bone structures (VBSs) and intervertebral discs (IVDs) for all data samples were segmented manually by a skilled surgeon and served as the "ground truth." After data preprocessing, a 3D-UNet model based on deep learning was used for automated segmentation of lumbar spine structures at L5/S1 level magnetic resonance imaging (MRI). Segmentation performances and morphometric measurement were used for 3D lumbosacral intervertebral foramen (LIVF) reconstruction generated by either manual segmentation and automatic segmentation.

Results: The 3D-UNet model showed high performance in automatic segmentation of lumbar spinal structures (VBSs and IVDs). The corresponding mean Dice similarity coefficient (DSC) of 5-fold cross-validation scores for L5 vertebrae, IVDs, S1 vertebrae, and all L5/S1 level spinal structures were $93.46 \pm 2.93\%$, $90.39 \pm 6.22\%$, $93.32 \pm 1.51\%$, and $92.39 \pm 2.82\%$, respectively. Notably, the analysis showed no associated difference in morphometric measurements between the manual and automatic segmentation at the L5/S1 level.

Limitations: Semantic segmentation of multiple spinal structures (such as VBSs, IVDs, blood vessels, muscles, and ligaments) was simultaneously not integrated into the deep-learning method in this study. In addition, large clinical experiments are needed to evaluate the clinical efficacy of the model.

Conclusion: The 3D-UNet model developed in this study based on deep learning can effectively and simultaneously segment VBSs and IVDs at L5/S1 level from MR images, thereby enabling rapid and accurate 3D reconstruction of LIVF models. The method can be used to segment VBSs and IVDs of spinal structures on MR images within near-human expert performance; therefore, it is reliable for reconstructing LIVF for L5/S1 LTRFA.

Key words: Deep learning, automatic segmentation, manual segmentation, lumbosacral intervertebral foramen, vertebral bone structures, intervertebral discs, 3D-UNet model, MRI, 3D reconstruction

Pain Physician 2022; 25:E27-E35

Degenerative disc disease is a leading cause of chronic back pain in the aging population worldwide (1). Lumbar transforaminal radiofrequency ablation (LTRFA), such as percutaneous nucleoplasty, uses radiofrequency and transforaminal laser ablation of the sinuvertebral nerve (Fig. 1) and is a minimally invasive intervention widely used (2,3) to treat chronic back pain. These approaches have the advantages of avoidance of general anesthesia, a shorter hospital stay, preservation of spinal stability, and an unencumbered ability to subsequently perform conventional open disc surgery (4-6).

In these procedures, the first step requires an accurate needle puncture in small sinuvertebral nerve fibers of the superficial annulus of the pathological disc (7). This process is important because it guides the bipolar radiofrequency probe to the right targeted treatment area (Fig. 2) (6). Currently, LTRFA under 2-dimensional (2D) images guidance (fluoroscopic or CT) are widely used to improve the accuracy and safety of this procedure (8). However, the cranial-caudal, lateral-medial, dorsal-ventral transforaminal approach was relatively strange to many spine surgeons due to lumbar intervertebral foramen and the puncture trajectory being 3-dimensional (3D) (9), mainly at the L5/S1 disc level, which exhibits some anatomical limitations such as narrow foraminal area (FA) and transverse process hypertrophy. It then leads to a greater possibility of bony structure obstruction and makes the probe entry into the spinal canal challenging. Therefore, Huang and Chen proposed a preoperative 3D planning method to find an ideal trajectory for the transforaminal procedure (9,10). A 3D method was developed to accurately

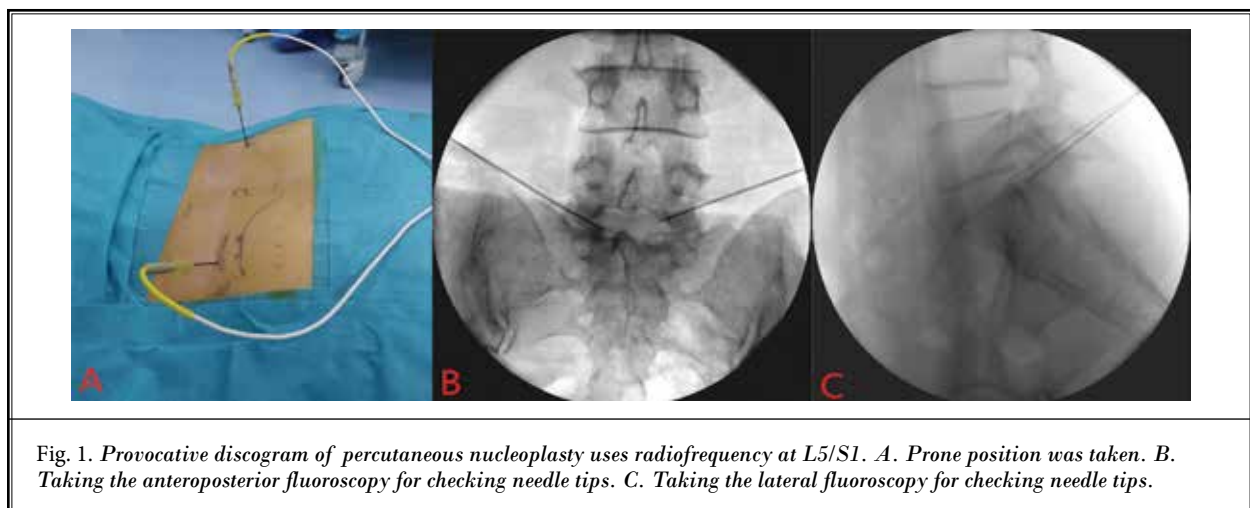
explore the relationship between the trajectory and 3D lumbar intervertebral foramen. However, manual segmentation of lumbar anatomical structures for 3D lumbosacral intervertebral foramen (LIVF) reconstruction is labor-intensive and time-consuming.

Automatic segmentation based on deep learning for medical images has the advantage of high efficiency and fast speed. It has been developed in many clinical setups. Automatic segmentation based on the deep-learning model has been used for measurement of leg length discrepancy (11), in the planning of the surgical treatment (12), and in the diagnosis of osteoarthritis (13,14). Studies report that automated segmentation of the anatomical structures of medical images can be performed rapidly by a deep learning algorithm. Automated segmentation helps make more efficient use of doctors' time and expertise (15). To the best of our knowledge, studies have not explored automatic segmentation of lumbar structures, including intervertebral bone structures (VBSs) and intervertebral discs (IVDs) at the L5/S1 level of axial magnetic resonance imaging (MRI). Therefore, this study sought to develop an automatic segmentation model based on a deep-learning algorithm to generate a 3D LIVF model. The model developed in this study can help doctors in planning an ideal trajectory effectively and rapidly in 3D image-guided interventional procedures at the L5/S1 disc level.

METHODS

Study Patients and Dataset

Institutional Board Review and the ethics commit-



tee of our hospital (IRB number: 2020 K05-1) approved this study. All patients signed an informed consent form. A total of 100 L5/S1 level data samples from 100 study patients were collected from March 2020 to July 2020 at our hospital. The inclusion criteria were as follows: (1) patients age > 18 years of age; (2) No contraindication for magnetic resonance (MR) examination. The exclusion criteria were as follows: 1) previous spinal surgery; 2) congenital abnormalities; 3) lumbar spondylolisthesis, instability, or malformation; 4) other severe mental and physical diseases, active infection, and pregnancy. All axial MR images were generated with a 3T MR unit (Magnetom Verio; Siemens, Erlangen, Germany) using 3D isotropic T2-weighted TSE sampling perfection with optimized contrasts using different flip angle evolution (3D T2W SPACE) sequence (16). The 3D T2W SPACE was performed using MRI parameters including TR 2800 ms, TE 189 ms, slice thickness 0.8 mm, matrix 320 × 320, flip angle 45°, and acquisition time was approximately 8 minutes per section.

Manual Segmentation and Data Preprocessing

All axial MR images were manually segmented with Mimics Innovation Suite® 19 software (Materialise, Inc., Leuven, Belgium). All VBSs and IVDs of lumbosacral structures were marked and labeled on Mimics® software by a spine surgeon, who is an expert in reading lumbar MRI and had systematic training in Mimics®. Then the segmented marks were reviewed by an expert radiologist and another expert surgeon with more than 20 years of experience in reading lumbar MRI. Any disagreements of segmentation were voted by the 3 doctors, and these manual marks were regarded as the ground truth. Manual segmentation masks were saved and exported as NIfTI files.

All images were subjected to cropping, normalization, and padding preprocessing steps. More details of data preprocessing are described in the Supplementary Material.

Model Architecture and Experimental Configurations

A 3D U-shaped architecture known as 3D-UNet (17), which is favored in medical segmentation, was used for automated segmentation of lumbar spine structures. The 3D-UNet consisted of an encoder (the left path) and a decoder (the right path), as outlined in Supplemental Fig. E1. More details of the 3D-UNet model architecture are described in the Supplementary Material.

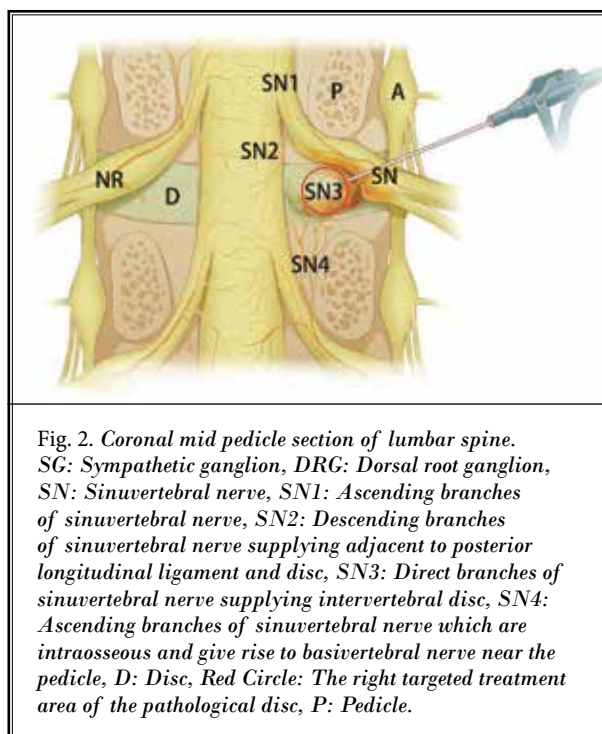


Fig. 2. Coronal mid pedicle section of lumbar spine. SG: Sympathetic ganglion, DRG: Dorsal root ganglion, SN: Sinuvertebral nerve, SN1: Ascending branches of sinuvertebral nerve, SN2: Descending branches of sinuvertebral nerve supplying adjacent to posterior longitudinal ligament and disc, SN3: Direct branches of sinuvertebral nerve supplying intervertebral disc, SN4: Ascending branches of sinuvertebral nerve which are intraosseous and give rise to basivertebral nerve near the pedicle, D: Disc, Red Circle: The right targeted treatment area of the pathological disc, P: Pedicle.

Five-fold cross-validation was used for performance evaluation and morphometry analysis. Detail of experimental configurations is shown in the Supplementary Material. The 3D-UNet was trained for about 7 hours using 3 RTX 2080Ti GPUs (Nvidia, Santa Clara, CA) using a parallel model and tested for about 2.5 s per subject using an RTX 2080Ti GPU.

Model Performances Evaluation and Morphometric Evaluation

Quantitative metrics, including Dice similarity coefficient (DSC), precision, and recall, were used to evaluate model performances of segmentation (18,19). The model for each dataset was generated for predicting L5 vertebra, S1 vertebra, and L5/S1 level disc. In addition, morphometric evaluation, including FA; foraminal height (FH); and foraminal width (FW) of 3D LIVF (Fig. 3), was used as validation for the precision of the automatic segmentation longitudinally. FA was measured based on the VBSs and IVDs boundary of 3D LIVF; FH was defined as the longest distance between the cranio-caudal boundary, and FW was defined as the shortest distance between the postero-inferior corner of proximal vertebrae and the opposing boundary (20). Two independent investigators evaluated these morphometric parameters of 3D LIVF models generated from automatic segmentation and manual segmentation. One of the investiga-

tors repeated measurement of these morphometric parameters for 3D LIVF models. The test-retest reliability and interobserver reliability of morphometric measurement were evaluated using the intraclass correlation coefficient (ICC). An ICC of 0.6-0.8 was considered good agreement, and an ICC greater than 0.8 was considered excellent based on Landis' definition (21).

Statistical Analysis

Morphometric measurement of 3D LIVF models was evaluated using Pearson correlation coefficient (R) and Wilcoxon signed-rank test to assess the correlation between automatic segmentation and manual segmentation for the longitudinal validation. Scatterplots and Bland-Altman plots were used to analyze linear relationships and correlation across L5 vertebrae, S1 vertebrae, and L5/S1 level disc of the test dataset between automatic segmentation and manual segmentation.

All statistical tests were performed using SPSS Version 26.0 (IBM Corporation, Chicago, USA). $P \geq 0.05$ represented no significant difference between automatic segmentation and manual segmentation of 3D LIVF models. $P < 0.05$ represented a significant difference in morphometric measurement between automatic segmentation and manual segmentation.



Fig. 3. LIVF dimensions were measured at the lateral views. LIVF height (FH) was defined as the longest distance between the cranio-caudal boundary (green line); the width (FW) was defined as the shortest distance between the postero-inferior corner of the proximal vertebrae and the opposing boundary (blue line), and the area (EA) was drawn with the temporary boundaries set at 0.5 mm increments (red circle) based on the 3D LIVF model outline (red line).

RESULTS

Patient Characteristics

A total of 100 L5/S1 levels from 100 patients were used in the final analysis. Age of patients ranged from 23 to 84 years (average, 39.2 years). Body mass index of patients ranged from 16.02 to 33.03 kg/m² (average, 23.28 kg/m²).

Segmentation Performances and Speed of 3D-UNet Model

Evaluation results (including the training, validation, and test datasets results) of the segmentation model are presented in Table 1. The 3D-UNet model achieved accurate segmentation of spine structures (L5 vertebrae, IVDs, S1 vertebrae, and all L5/S1 level spinal structures segmentation) on axial MR images, as shown in Fig. 4. The corresponding mean DSC of 5-fold cross-validation scores of test datasets for L5 vertebrae, IVDs, S1 vertebrae, and all L5/S1 level spinal structures were $93.46 \pm 2.93\%$, $90.39 \pm 6.22\%$, $93.32 \pm 1.51\%$, and $92.39 \pm 2.82\%$, respectively. The corresponding mean precision of 5-fold cross-validation scores of test datasets for L5 vertebrae, IVDs, S1 vertebrae, and all L5/S1 level spinal structures were $94.15 \pm 4.35\%$, $90.59 \pm 6.17\%$, $93.79 \pm 2.92\%$, and $92.85 \pm 2.73\%$, respectively. The corresponding mean recall of 5-fold cross-validation scores of test datasets for L5 vertebrae, IVDs, S1 vertebrae, and all L5/S1 level spinal structures were $92.95 \pm 3.01\%$, $91.00 \pm 8.32\%$, $93.00 \pm 3.03\%$, and $92.31 \pm 3.57\%$, respectively. Notably, a skilled doctor took about 6 hours per single case to complete the manual segmentation task of images, whereas the 3D-UNet model takes about 2.5 seconds to finish an automatic segmentation on a single case after training.

Morphometric Analysis of 3D LIVF Models

Morphometric analysis of 3D reconstruction LIVF models generated from manual segmentation (Fig. 5A) and automatic segmentation (Fig. 5B) were evaluated. A full breakdown of these morphologic metrics, including FA; FH; and FW, are presented in Table 2 and scatterplots and Bland-Altman plots shown in Fig. 6. Morphometric metrics showed strong test-retest reliability and interobserver reliability between manual segmentation and automatic segmentation (Table 3).

DISCUSSION

Information on geometric anatomy of 3D LIVF is essential for ensuring accurate needle puncture in the right targeted treatment area of the pathological

disc when performing LTRFA (6,8). However, 3D LIVF based on manual segmentation is time-consuming. In addition, 3D LIVF model based on automatic segmentation has never been explored for use in performing LTRFA. Deep learning can generate 3D LIVF models rapidly and accurately with the help of automatic segmentation, which is crucial for the planning of surgical treatment in orthopedics. This study explored the feasibility of automatic segmenting lumbosacral structures (VBSs and IVDs) on axial MRI through deep learning and 3D reconstruction of LIVF.

3D reconstruction of LIVF can improve viability assessment of LTRFA, especially at the L5/S1 level. The needle trajectory is directed on the right region, at the region of the herniated portion, and pathological neurotization of sinuvertebral nerves (4,6,22). However, trajectory planning guided with 2D images is difficult at the L5/S1 level in some cases due to anatomy obstacles such as narrow foraminal area, the hypertrophic L5-S1 facet joint, and transverse process hypertrophy (23). For LTRFA, 3D surgical planning is more conducive to 2D surgical planning, especially in the level of the lumbosacral intervertebral foramen. 3D methods have been developed to evaluate the preoperative trajectory for transforaminal approach quantitatively; however, these methods have some limitations. Firstly, they are complex and difficult to understand for preoperative trajectory planning methods evaluated through the axial, sagittal, and coronal slices simultaneously (23,24). Moreover, 3D reconstruction of lumbar models is mainly rendered by computerized tomography (CT) images (9,10). Additional radiation exposure during CT examination may pose adverse effects in patients, and the CT image cannot clearly show the herniated portion. In addition, 3D-rendering LIVF models reconstructed by manual segmentation is time-consuming. Instead, the 3D LIVF model generated in our study from automatic segmentation on axial MR images took approximately 2.5 seconds and quickly provided the specific perspective with the right region.

The deep learning algorithm model developed in this study showed high performance in the segmentation of lumbar structures (VBSs and IVDs) and can rapidly and precisely reconstruct the 3D LIVF model at L5/S1 level. Previous segmentation algorithms achieved simultaneous volumetric segmentation of VBSs and IVDs on sagittal MR images. Fallah et al's (25) approach achieved a DSC of 92.5% for VBSs segmentation and 91.4% for IVDs segmentation. Li et al (26) reported DSCs of 88.01% and 92.59% for VBSs and IVDs, respectively. A previous study performed by our team reported a DSC of 87.32% for VBSs segmentation and 87.78% for IVDs segmentation (27). However, the previous approaches could not segment vertebral bone structures effectively and could not be used to reconstruct 3D LIVF models effectively. In the present study, simultaneous volumetric segmentation of VBSs and IVDs on axial MR images was

Table 1. Results of automatic segmentation performances according to the dataset.

Performances and Dataset	DSC			Precision			Recall		
	VBSs	IVDs	VBSs and IVDs	VBSs	IVDs	VBSs and IVDs	VBSs	IVDs	VBSs and IVDs
Training	0.953 (0.953, 0.954)	0.935 (0.933, 0.936)	0.947 (0.946, 0.948)	0.956 (0.955, 0.957)	0.928 (0.925, 0.931)	0.947 (0.946, 0.948)	0.951 (0.950, 0.952)	0.942 (0.940, 0.945)	0.948 (0.947, 0.949)
Validation	0.933 (0.929, 0.936)	0.901 (0.883, 0.920)	0.922 (0.915, 0.930)	0.938 (0.932, 0.943)	0.893 (0.862, 0.924)	0.923 (0.913, 0.933)	0.929 (0.923, 0.935)	0.920 (0.908, 0.931)	0.926 (0.919, 0.932)
Test	0.934 (0.931, 0.937)	0.904 (0.892, 0.916)	0.924 (0.918, 0.930)	0.940 (0.935, 0.945)	0.906 (0.894, 0.919)	0.928 (0.923, 0.934)	0.930 (0.926, 0.934)	0.910 (0.893, 0.926)	0.923 (0.916, 0.930)

Note. — Data are means of 5-Fold Cross-validation scores, with 95% confidence intervals in parentheses. DSC = Dice similarity coefficient, VBSs = vertebra bone structures (L5 vertebrae and S1 vertebrae), IVDs = intervertebral discs.

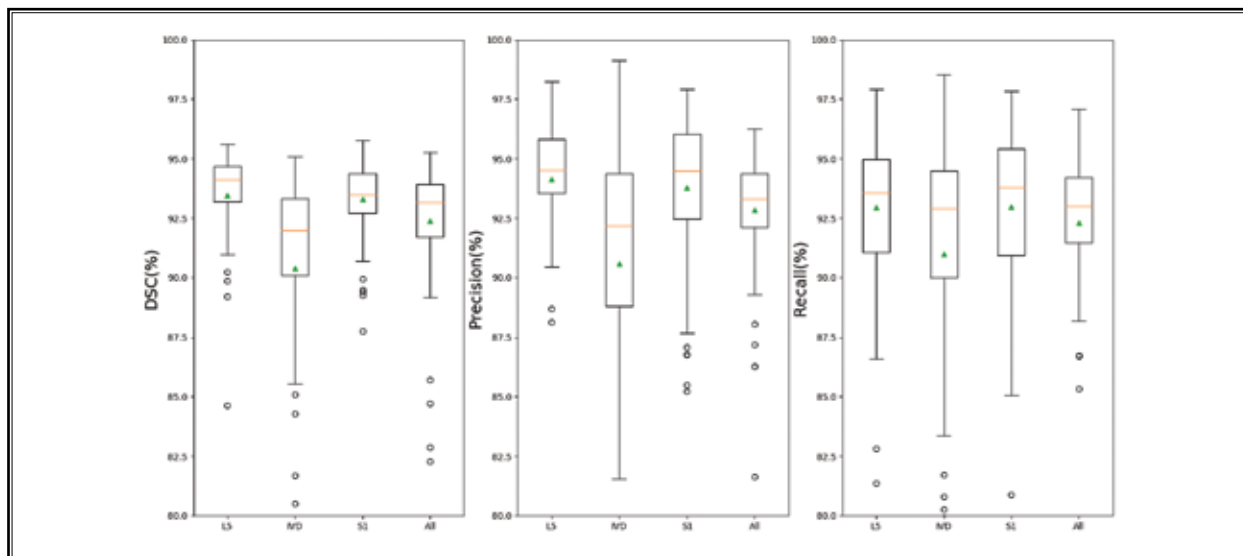


Fig. 4. The 3D-UNet model achieves high performance in terms of DSC, precision, and recall for segmentation of L5 vertebrae, IVDs, S1 vertebrae, and all 3 spinal structures at L5/S1 level. The orange line and green triangle in the box denote the median value and mean value, respectively.

Table 2. Results of morphology analysis according to L5/S1 test dataset.

Morphometric Parameters	Automatic Segmentation	Manual Segmentation	R value	P value
FA (mm ³)	107.826	108.703	0.972	0.202
FH (mm)	15.7167	15.7855	0.934	0.190
FW (mm)	6.9119	6.9903	0.844	0.254

Note.— Statistical significance is determined at the $P < 0.05$ level. FA = foraminal area, FH = foraminal height, FW = foraminal width.

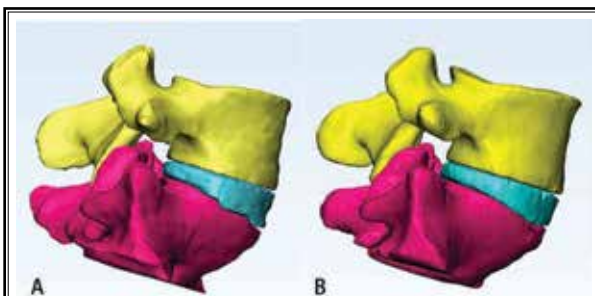


Fig. 5. A representative of 3D L5/S1 LIVF models at L5/S1 level showing a comparison between manual segmentation: A, and automatic segmentation: B, predicted using the 3D-UNet convolutional neural network. A, B in right views.

achieved, with high performance (VBSs DSC: 93.39% and IVDs DSC: 90.59%).

In addition, 3D reconstruction LIVF models were successfully achieved, as the approach considered segmentation of the superior and inferior articular processes. These vertebrae bone structures are important for the 3D reconstruction LIVF model, which comprises vertebral bodies, intervertebral disc, and the superior and inferior articular processes (28). 3D reconstruction models generated in this study can be used to quantify morphometric parameters of LIVF at L5/S1 level. Analysis of morphometric parameters including FA, FH, FW, showed no associated difference in morphometric measurements at the L5/S1 level between the manual and automatic segmentations.

The normal entrance point of transforaminal approaches was located at the L5/S1 level at 12 to 16 cm from the midline based on the size, gender, and level of the patient (29). The model generated through automatic segmentation algorithm can be used to evaluate the needle entry point and the needle entry angle accurately and rapidly in L5/S1 LTRFA as it can easily be modified, thus avoiding the above-mentioned anatomical obstacles. LIVF are filled with nerves and blood vessels (30) and are split into compartments by ligaments (31). The exiting nerve and blood vessels should be avoided during trajectory planning. Spinal nerves exit the spinal canal through the superior part of the LIVF (32), along with the associative blood vessels, and

veins run along the margin of the superior and inferior vertebral pedicle (30). The distribution of the exiting nerve and blood vessels in the LIVF has a regular anatomical pattern in normal anatomy. Still these anatomy structures may be changed in the majority of patients. While the MR reconstruction images in this study did not directly show the exiting nerve and blood vessels directly, the 3D LIVF model may be helpful to plan ideal trajectory in L5/S1 LTRFA, combined with 2D images.

This study had several limitations. First, to compare with CT scan, although MRI has the advantages of imaging-clear in soft tissue and radiation-free, MRI-based 3D model does come at a higher economic cost. In addition, only the L5/S1 level of patients was evaluated, whereas other levels of the spine were not included. Furthermore, although the exiting nerve and blood vessels surrounding the LIVF are crucial for L5/S1 LTRFA, these spinal structures were not segmented because showing these spinal structures accurately requires multimodal MR images. Further studies should explore multimodal MR or CT fusion techniques to solve the problem. Semantic segmentation of multiple spinal structures (such as VBs, IVDs, blood vessels, muscles, and ligaments) should be integrated into the deep-learning algorithm simultaneously in further studies.

CONCLUSIONS

In summary, the 3D-UNet model reported in this study based on deep learning can effectively segment VBs and IVDs on MR images simultaneously and can rapidly and accurately reconstruct 3D LIVF models. The findings of this study indicate that the proposed method can be used to segment VBs and IVDs of spinal structures on MR images within near-human expert performance, which is reliable for reconstructing LIVF for L5/S1 LTRFA.

Funding

Study supported by Zhuhai City Innovation and Innovation Team Project, Guangdong Province, China (ZH0406190031PWC), the National Natural Science Foundation of China (No. 62001207), China Postdoctoral Science Foundation (No. 2019M663269, Guangdong

Table 3. Reliability test of morphometric measurements of LIVF on 3D models.

Morphometric Parameters	FA		FH		FW	
	Test-retest Reliability	Inter-observer Reliability	Test-retest Reliability	Inter-observer Reliability	Test-retest Reliability	Inter-observer Reliability
Automatic Segmentation	0.995	0.995	0.973	0.961	0.981	0.987
Manual Segmentation	0.995	0.997	0.994	0.996	0.990	0.978

Note.— The level of agreement was interpreted as slight if ICC coefficient was 0 to 0.20; fair, 0.21 to 0.40; moderate, 0.41 to 0.60; substantial, 0.61 to 0.80; and almost perfect, 0.81 to 1. LIVF = lumbar intervertebral foramen.

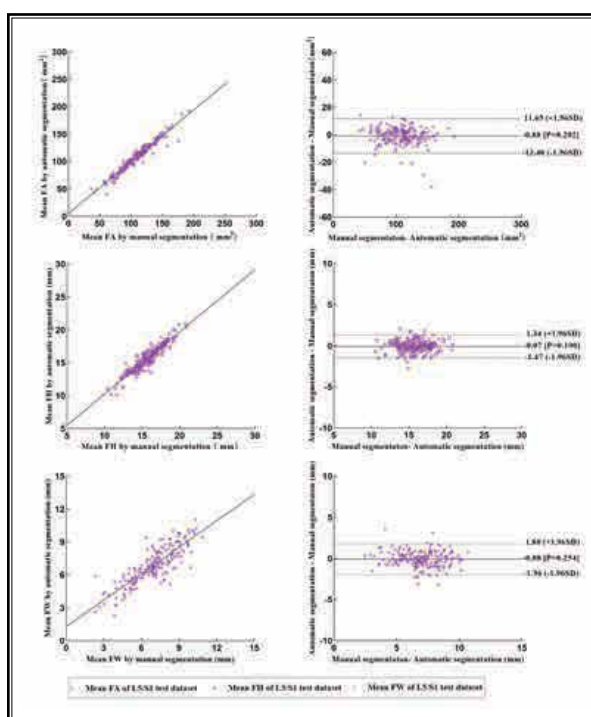


Fig. 6. Scatterplots and Bland-Altman plots showing FA measurements of test dataset (top), and FH measurements of test dataset (mid) FW measurements of test dataset (bottom) produced from manual and automatic segmentation methods. FA = foraminal area, Fh = foraminal height, FA = foraminal width.

Province Basic and Applied Basic Research Fund (No. 2019A1515110393), and by the Fundamental Research Funds for the Central Universities, Sun Yat-sen University (No. 20ykpy49).

Acknowledgments

Zheng Liu, Zhihai Su, and Min Wang contributed equally to this work and should be considered co-first

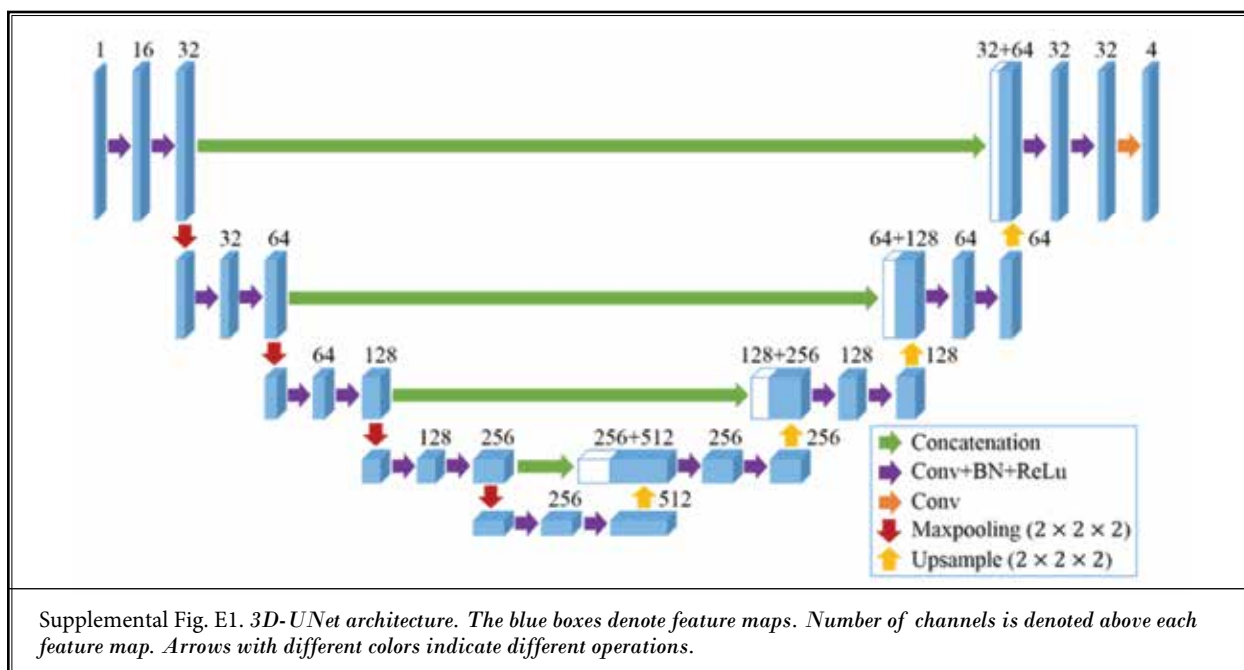
authors. Hai Lu and Shumao Pang contributed equally to this work. Hai Lu is the corresponding author. We gratefully acknowledge the support of the Home for Researchers editorial team ([www.home-for-research-](http://www.home-for-research-ers.com)

[ers.com](http://www.home-for-research-ers.com)), who provides a language editing service for this research, and Han Liu, who provides a diagram drawing service for this research.

REFERENCES

- Vos T, Flaxman AD, Naghavi M, et al. Years lived with disability (YLDs) for 1160 sequelae of 289 diseases and injuries 1990-2010: A systematic analysis for the Global Burden of Disease Study 2010. *Lancet* 2012; 380:2163-2196.
- Manchikanti L, Hirsch JA, Pampati V, Boswell MV. Utilization of facet joint and sacroiliac joint interventions in Medicare population from 2000 to 2014: explosive growth continues! *Curr Pain Headache Rep* 2016; 20:58.
- Starr JB, Gold L, McCormick Z, Suri P, Friedly J. Trends in lumbar radiofrequency ablation utilization from 2007 to 2016. *Spine J* 2019; 19:1019-1028.
- Ji GY, Lee J, Lee SW, et al. Safety and Effectiveness of transforaminal epiduroscopic laser ablation in single level disc disease: A case-control study. *Pain Physician* 2018; 21:E643-E650.
- Bjorland S, Moen A, Schistad E, Gjerstad J, Røe C. Genes associated with persistent lumbar radicular pain; A systematic review. *BMC Musculoskeletal Disord* 2016; 17:500.
- Kim HS, Wu PH, Jang IT. Lumbar degenerative disease part 1: Anatomy and pathophysiology of intervertebral discogenic pain and radiofrequency ablation of basivertebral and sinuvertebral nerve treatment for chronic discogenic back pain: A prospective case series and review of literature. *Int J Mol Sci* 2020; 21:1483.
- Mirzai H, Tekin I, Yaman O, Bursali A. The results of nucleoplasty in patients with lumbar herniated disc: A prospective clinical study of 52 consecutive patients. *Spine J* 2007; 7:88-93.
- Kim HS, Paudel B, Chung SK, Jang JS, Oh SH, Jang IT. Transforaminal epiduroscopic laser ablation of sinuvertebral nerve in patients with chronic discogenic back pain: Technical note and preliminary result. *J Neurol Surg A Cent Eur Neurosurg* 2017; 78:529-534.
- Huang X, Zhu B, Liu X. Quantitative 3D trajectory measurement for percutaneous endoscopic lumbar discectomy. *Pain Physician* 2018; 21:E355-E365.
- Chen X, Cheng J, Gu X, Sun Y, Politis C. Development of preoperative planning software for transforaminal endoscopic surgery and the guidance for clinical applications. *Int J Comput Assist Radiol Surg* 2016; 11:613-620.
- Liu F, Zhou Z, Jang H, Samsonov A, Zhao G, Kijowski R. Deep convolutional neural network and 3D deformable approach for tissue segmentation in musculoskeletal magnetic resonance imaging. *Magn Reson Med* 2018; 79:2379-2391.
- Moldovan F, Gligor A, Bataga T. Structured Integration and Alignment Algorithm: A Tool for Personalized Surgical Treatment of Tibial Plateau Fractures. *J Pers Med* 2021; 11.
- Norman B, Pedoia V, Majumdar S. Use of 2D U-net convolutional neural networks for automated cartilage and meniscus segmentation of knee MR imaging data to determine relaxometry and morphometry. *Radiology* 2018; 288:177-185.
- von Schacky CE, Sohn JH, Liu F, et al. Development and validation of a multitask deep learning model for severity grading of hip osteoarthritis features on radiographs. *Radiology* 2020; 295:136-145.
- Zheng Q, Shellikeri S, Huang H, Hwang M, Sze RW. Deep learning measurement of leg length discrepancy in children based on radiographs. *Radiology* 2020; 296:152-158.
- Sayah A, Jay AK, Toaff JS, Makariou EV, Berkowitz F. Effectiveness of a rapid lumbar spine MRI protocol using 3D T2-weighted SPACE imaging versus A standard protocol for evaluation of degenerative changes of the lumbar spine. *AJR Am J Roentgenol* 2016; 207:614-620.
- Wang C, Guo Y, Chen W, Yu Z. Fully automatic intervertebral disc segmentation using multimodal 3D U-Net, 2019 *IEEE 43rd Annual Computer Software and Applications Conference (COMPSAC)*, 2019, pp 730-739.
- Pang S, Lu Z, Jiang J, et al. Hippocampus segmentation based on iterative local linear mapping with representative and local structure-preserved feature embedding. *IEEE Trans Med Imaging* 2019; 38:2271-2280.
- Zou KH, Warfield SK, Bharatha A, et al. Statistical validation of image segmentation quality based on a spatial overlap index. *Acad Radiol* 2004; 11:178-189.
- Zhong W, Driscoll SJ, Tsai TY, et al. In vivo dynamic changes of dimensions in the lumbar intervertebral foramen. *Spine J* 2015; 15:1653-1659.
- Landis JR, Koch GG. The measurement of observer agreement for categorical data. *Biometrics* 1977; 33:159-174.
- Park CH, Lee SH. Endoscopic epidural laser decompression versus transforaminal epiduroscopic laser annuloplasty for lumbar disc herniation: A prospective, randomized trial. *Pain Physician* 2017; 20:663-670.
- Eun SS, Lee SH, Liu WC, Erken HY. A novel preoperative trajectory evaluation method for L5-S1 transforaminal percutaneous endoscopic lumbar discectomy. *Spine J* 2018; 18:1286-1291.
- Tezuka F, Sakai T, Abe M, et al. Anatomical considerations of the iliac crest on percutaneous endoscopic discectomy using a transforaminal approach. *Spine J* 2017; 17:1875-1880.
- Fallah F, Walter SS, Bamberg F, Yang B. Simultaneous volumetric segmentation of vertebral bodies and intervertebral discs on fat-water MR images. *IEEE J Biomed Health Inform* 2019; 23:1692-1701.
- Li T, Wei B, Cong J, et al. S3egANet: 3D spinal structures segmentation via adversarial nets. *IEEE Access* 2020; 8:1892-1901.
- Pang S, Pang C, Zhao L, et al. SpineParseNet: spine parsing for volumetric MR image by a two-stage segmentation framework with semantic image representation. *IEEE Trans Med Imaging* 2021; 40:262-273.
- Gilchrist RV, Slipman CW, Bhagia SM. Anatomy of the intervertebral foramen. *Pain Physician* 2002; 5:372-378.

29. Hoogland T, van den Brekel-Dijkstra K, Schubert M, Miklitz B. Endoscopic transforaminal discectomy for recurrent lumbar disc herniation: A prospective, cohort evaluation of 262 consecutive cases. *Spine* 2008; 33:973-978.
30. Su Z, Wang M, Zhao Q, et al. Clinical anatomy and possible clinical significance of the intervertebral vein in the lumbar intervertebral foramina. *Pain Physician* 2019; 22:E225-E232.
31. Yuan SG, Wen YL, Zhang P, Li YK. Ligament, nerve, and blood vessel anatomy of the lateral zone of the lumbar intervertebral foramina. *Int Orthop* 2015; 39:2135-2141.
32. Kambin P, Brager MD. Percutaneous posterolateral discectomy. Anatomy and mechanism. *Clin Orthop Relat Res* 1987; 145-154.



SUPPLEMENTAL MATERIALS:

Data Preprocessing:

Given an image $I \in \mathbb{R}^{D \times H \times W}$, the cropped image I_{crop} was acquired as follows:

$$I_{\text{crop}}(I) = I\left[: , \frac{1}{4}H - 10 : \frac{3}{4}H + 10, \frac{1}{4}W - 20 : \frac{3}{4}W\right]$$

where D , H , W denotes the depth, height, and width of the image, respectively. In our dataset, $H = W = 320$ and D varied between 88 and 128. Ultimately, the cropped image size was $D \times 100 \times 100$, which were then normalized by subtracting the average of the voxels and dividing their standard deviations. The normalized images were eventually padded with zeros to $128 \times 180 \times 180$.

Model Architecture:

The input of 3D-UNet was a $128 \times 180 \times 180$ MR image with a channel. The 3D-UNet output had 4 channels, denoting the probability that each voxel belongs to the background, upper vertebra, IVD, and lower vertebra. For L5/S1 level images, the upper vertebra and lower vertebra represented L5 vertebra and S1 vertebra, respectively. The size of convolutional kernels was $3 \times 3 \times 3$ except for the last convolutional layer, which used a $1 \times 1 \times 1$ convolutional kernel. The upsample module was implemented through trilinear interpolation.

Experimental Configurations:

Each dataset was randomly categorized into 5 groups, each group with 20 study samples. Four groups containing 80 samples were used as the training set for the automated segmentation model. The other group containing 20 samples served as the test dataset. During training, 10 samples were randomly selected for validation. For each experiment, the training, validation, and test datasets comprised 70, 10, and 20 samples, respectively. This procedure was conducted in five replicates until the segmentation results of all samples were obtained. 3D-UNet, implemented by Pytorch version 1.5.1 (open-source, Facebook Artificial Intelligence Research), was trained with a batch size of 2 for 100 epochs using Adam optimizer. The learning rate was initially set at 0.0005 and then lowered by 5 times at epoch 33 and 66.